Electromagnetic incremental assembly for large thin-walled ring shells and microscopic mechanisms of dynamic deformation overlap regions

X. Cheng[1], H. P. Yu[1,2,3,*], J. P. Guo[1,3], H. Wang[1], T.S. Yu[4]

[1] School of Materials Science and Engineering, Harbin Institute of Technology, China
[2] National Key Laboratory for Precision Hot Processing of Metals, Harbin Institute of Technology, China
[3] Suzhou Research Institute, Harbin Institute of Technology, China
[4] Jilin Provincial Civil Aviation Airport Group Co., Ltd., China
*Corresponding author. Email: haipingy@hit.edu.cn

Abstract

This paper introduced an electromagnetic incremental assembly (EMIA) method which employed large thin-walled aluminum alloy ring shells as the processing object and a weak-rigidity assembled structure with an irregular cross-section as the support object. By experiments, the effects of discharge frequency, discharge voltage, and coil position parameters on the assembly outcome were investigated. The results show that this method successfully achieved a tight fit between the skin and the assembled structure, as well as effective support. During the EMIA, there were many two-step dynamic deformation overlap regions. This paper also conducted an in-depth study on the microstructure evolution of these deformation overlap regions, revealing that dynamic pre-forming enhanced the strength and plasticity of the material. The enhanced strength was attributed to the higher dislocation density within grain boundaries. The plasticity enhancement was mainly due to two factors: firstly, the more uniform dislocation distributions which promoted homogeneous deformation; secondly, the shear stress on the second-phase particles became more concentrated, and the shear action was enhanced. As a result, a large number of original particles were sheared into multiple segments, and large-scaled particles were also fractured, leading to the accumulation of dislocations that eventually cut through the particles, releasing local shear stress.

Keywords

Large thin-walled ring shells, Electromagnetic incremental assembly, Microstructure evolution

1 Introduction

Thin-walled ring shells are a classic type of thin-walled structure characterized by a significant disparity between wall thickness and radial dimensions. In modern manufacturing for aerospace, electromechanical systems, and engineering machinery, there is a growing demand for high-precision ring shells with specific cross-sectional profile. For some structurally unstable assembly components that require support, employing thin-walled metal shells as inner lining support structures not only provides stable assembly support but also reduces the overall system weight. For instance, a sandwich tube consists of an inner tube, outer tube and core layer, and experiences minimal deformation under external forces (Huang et al., 2022). However, the thin-walled liners are typically made of lightweight, high-strength, low-formability materials, which pose challenges due to their low structural stiffness and closed processing environments, limiting the applicability of traditional processing methods.

Compared to traditional forming processes, the advantages of electromagnetic forming (EMF) in manufacturing thin-walled ring shells lie in its high strain rate characteristics, which can reduce springback and increase the material's forming limit at room temperature (Psyk et al., 2011). Additionally, as a replacement for traditional punch, the coil structure offers strong adaptability. It can be adjusted according to the part structure, thus overcoming limitations imposed by the processing environments (Cheng and Yu, 2025). Electromagnetic incremental forming (EMIF) is an extended processing form of traditional EMF. By combining multi-step discharges from coil with incremental movement, the EMIF enables the processing of large-scaled sheets and long straight tubes (Cui et al., 2014). Based on the concept of EMIF, this paper introduced a novel incremental processing method—electromagnetic incremental assembly (EMIA). For the assembled structure of rigid polyurethane foam (RPUF) blocks with large-scaled and irregular cross-sectional features, radial support assembly was achieved through the EMIF of large aluminum alloy thin-walled ring skins, allowing the skin and the RPUFs to form an integrated whole and ensuring the stability of the assembled structure. The working principle of EMIA was introduced. By conducting multi-step incremental discharge experiments, the effects of discharge voltage, discharge frequency, and coil positions on the assembly outcome were analyzed. The optimal process parameter scheme was obtained, and the feasibility of EMIA was verified.

In the EMIA process, due to the overlapping of coil incremental positions, there are significant dynamic deformation overlap regions in the skin material. Considering the processing efficiency, the coil overlap between the front and rear discharge steps should not exceed 50%. Therefore, the deformation overlap regions generally undergoes two discharges. influenced by dynamic pre-forming, the mechanical properties and microstructural evolution in the deformation overlap regions may differ compared to fully dynamic deformation regions. This paper also investigated the effect of dynamic pre-forming on the material forming performance and microstructural evolution under two-step dynamic deformation. The mechanical properties and microscopic mechanisms of aluminum alloy under fully and two-step dynamic deformations were analyzed.

2 Electromagnetic incremental assembly

2.1 Working principle

Fig. 1 illustrates the working principle of EMIA for thin-walled ring shells, which consists of four components: thin-walled ring shell, assembly block, coil, and die. The assembly blocks are radially supported by the shell through EMIF. The process flow is as follows:

(1) The thin-walled ring shell is positioned and installed coaxially with the assembly blocks or die, ensuring that the gap between the shell and the assembly blocks is uniform.

(2) After setting the discharge voltage, perform the single-step discharge forming to achieve the local tight fitting between the shell and the assembly blocks.

(3) Keep the position of the shell fixed relative to the assembly blocks, and move the coil along the axial direction with the preset feed distance, so that the undeformed region of the shell enters the forming region of the coil. After setting the discharge voltage, perform the discharge machining again.

(4) Step (3) is repeated until the entire forming process of the shell is completed.

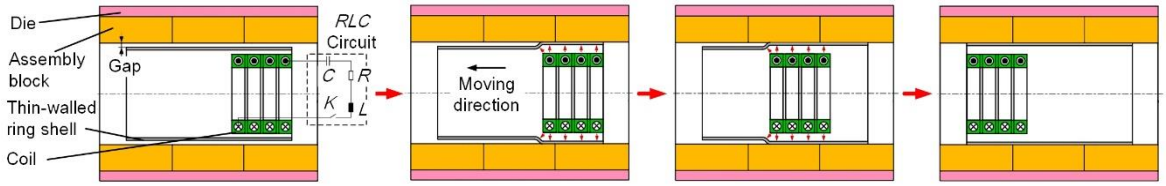

***Figure 1**: Working principle of EMIA*

2.2 Materials and experimental setup

The thin-walled ring shell material is 5A06 annealed aluminum alloy (AA5A06) skin. The shell is made from AA5A06 rolled sheet with a thickness of 1.5 mm, with overall dimensions of 600mm × 450mm × 72mm, and the weld seam is located at the bottom center. The materials of assembly blocks are RPUFs with a density of 200 kg/m³. **Fig. 2a** shows the experimental setup, which consists of four components: thin-walled ring skin, assembled RPUFs, coil, and die. The cross-section of the assembled foams consists of six foam pieces. The coil for irregular structure uses rectangular copper wire with cross-sectional dimensions of 5mm × 7mm, wound for 5 turns. The arc and straight-wall regions of die are made from steel plate with a thickness of 10 mm, which are bent and then welded to base plate with a thickness of 30 mm to form an integrated structure. The maximum stored energy of EMF device is 30 kJ, and the energy storage capacitor has a capacitance of 150 μF. The inductance of the pulse generator in the EMF device is 14.8 μH, and the current curve under a discharge voltage of 11.5 kV is shown in **Fig. 2b**.

The initial assembly between the skin, coil, and assembled RPUFs is shown in **Fig. 2c**. The assembled RPUFs are divided into the arc region, transition region, straight-wall region, and bottom region. The regions of skin that are closely fitted with the bottom and straight-wall regions of the foams do not participate in the bulging deformation. The deformation of the skin primarily affects the transition and arc regions of foams. The complex shape of

foams results in an uneven initial gap between the skin and the foam, with the maximum and minimum initial gaps occurring between the foam transition region and the skin.

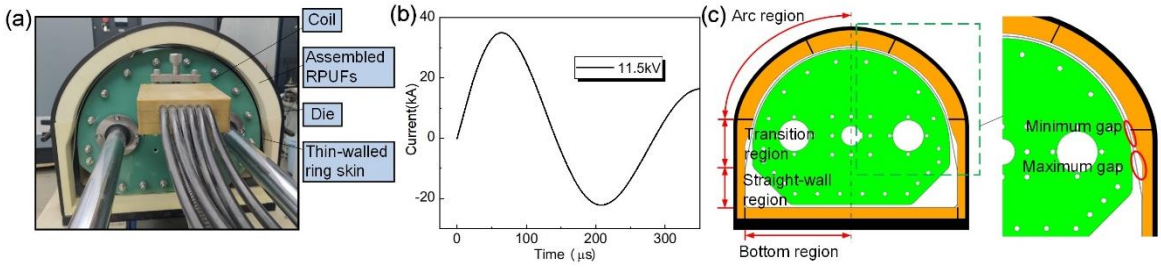

***Figure 2**: Experimental setup for EMIA* (a) experimental equipment, (b) current curve under a discharge voltage of 11.5 kV, (c) initial assembly

In the case where the initial gap between the skin and the foam is determined, the main adjustable process parameters include discharge voltage U, discharge frequency N, and coil position c. The coil position c is represented by the center distance between the skin and the coil, as shown in **Fig. 3**. U_1 represents the first-step discharge voltage, and c_1 represents the center distance during the first discharge, with other parameters expressed similarly.

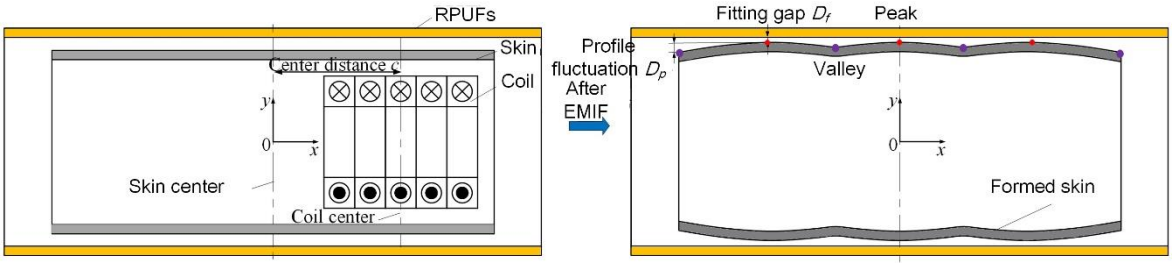

***Figure 3**: Assembly relationship between the coil, skin, and RPUFs*

From **Fig. 3**, when the coil moves incrementally over a large distance, the deformation overlap region becomes smaller, and the skin profile after EMIF may exhibit a wavy pattern. The fitting gap D_f between the formed skin and the foams, as well as the fluctuation D_p in the profile waves, will affect the supporting performance of the formed skin. Additionally, during the EMIA, it is crucial to prevent excessive impacts from damaging the foams.

To measure the profile of formed skin and calculate the profile fluctuation D_p, a Multi-Instrument is used to measure the skin profile along axial direction. The distance data between skin profile and sensor is collected at various points along measurement trajectory. Since the contact area between the formed skin and the foams' arc region is the largest, a linear trajectory is generally chosen for measurement at this location. If the skin undergoes three discharges, the skin profile shows three peaks and four valleys. The difference between the highest peak and the lowest valley is taken as the profile fluctuation D_p of formed skin.

2.3 Experiments

The EMIA experimental schemes were conducted by adjusting different process parameters, as shown in **Table 1**. The experimental results are shown in **Fig. 4**.

Table1 Experimental schemes of EMIA

Parameters	EMIA-1	EMIA-2	EMIA-3	EMIA-4	EMIA-5	EMIA-6
U_1/kV	8.5	8.5	11	11.5	11.5	11.5
c_1/mm	+28	0	0	0	0	0
U_2/kV	8.5	9.5	12	11.5	11.5	11.5
c_2/mm	-28	+20	+20	+20	+20	+23
U_3/kV	/	10	12	11.5	11.5	11.5
c_3/mm	/	-20	-20	-20	-20	-23
U_4/kV	/	/	/	/	11.5	/
c_4/mm	/	/	/	/	+25	/
N	2	3	3	3	4	3

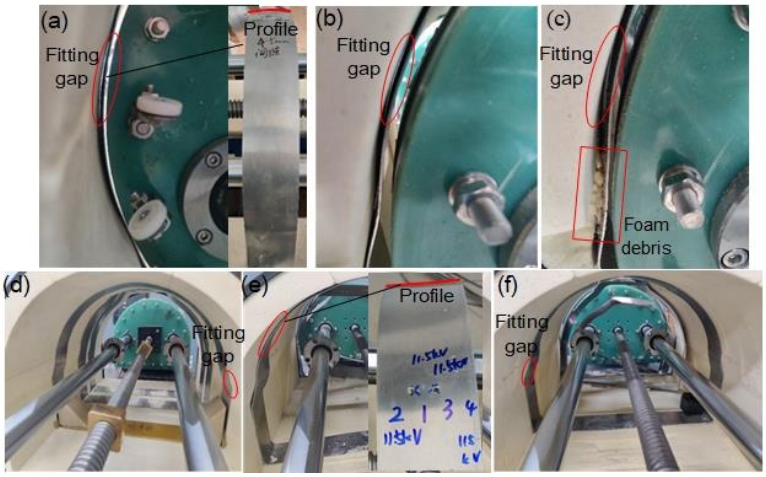

***Figure 4**: Results (a) EMIA-1 (b) EMIA-2 (c) EMIA-3 (d) EMIA-4 (e) EMIA-5 (f) EMIA-6*

From **Figs. 4a** and **4b**, there were obvious fitting gaps between the formed skin and the foams' arc region in EMIA-1 and EMIA-2, which indicated that the discharge voltage of 8-10 kV was too low, and the discharge voltage should be increased further to reduce the fitting gap. In EMIA-1, the profile of the formed skin showed a noticeable "high in the middle and low on both edges " phenomenon, leading to worse profile fluctuation. Therefore, two discharges were not suitable. EMIA-3 attempted to set the discharge voltage to 11 kV and 12 kV. When the discharge voltage was 11 kV, the foams remained intact. However, when the discharge voltage increased to 12kV, the convex feature of foams was crushed, and foam debris appeared, as shown in **Fig. 4c**. This indicated that a discharge voltage of 12kV was too high, and the enormous impact generated by the deformation of skin material led to the damage to foams. Therefore, the discharge voltage need to be slightly reduced. EMIA-4 and EMIA-6 differ only in the coil position for each step. From **Figs. 4d** and **4f**, the fitting effects of the formed skin were similar in both experiments. The skin fitted closely to the arc region of the foams, and there was no obvious damage to the foams. However, there was about a 2.5 mm fitting gap between the skin and foams' concave feature, which resulted from that the initial gap in this region was 11.5 mm, and under the discharge voltage of 11.5

kV, the deformation of skin material was insufficient to fill the concave feature. In EMIA-5, four discharges were performed under a discharge voltage of 11.5 kV. As shown in **Fig. 4e**, there was no fitting gap between the formed skin and the foams, but the profile fluctuation was poor. Since the last two discharges occurred on the right edge of the skin, it caused accumulated deformation on the right edge of skin, resulting in a noticeable upward warping. Therefore, during the EMIA, the coil discharge positions need to be arranged symmetrically around the skin center.

Based on the analyses of fitting effects in EMIA-1~6, the fitting gaps in EMIA-4 and EMIA-6 were minimum. Next, the profiles of the formed skins in EMIA-1~6 were measured. Although the formed skins in EMIA-4 and EMIA-6 both showed good fitting with the foams, the profile fluctuation of formed skin in EMIA-4 was only 0.57 mm, which indicates that the support stability of the formed skin in EMIA-4 was better than in EMIA-6. Therefore, the process parameters in EMIA-4 represented the optimal process scheme, which included three discharge with a discharge voltage of 11.5kV for each cycle, and a coil center spacing of 20 mm during each discharge.

3 Microscopic mechanisms of deformation overlap regions

During the EMIA, the skin material undergoes multiple discharges, resulting in dynamic deformation overlap regions. These overlap regions generally experiences two-step dynamic deformation. There may be differences in mechanical properties and microstructural evolution between the dynamic deformation overlap regions and the single-deformation region. Based on existing literature (Cheng, 2025), quasi-static pre-forming can improve the plasticity of subsequent dynamic deformation. Therefore, dynamic pre-forming may also affect subsequent dynamic deformation.

To investigate it, the mechanical properties of AA5A06 sheets were tested under fully and two-step dynamic uniaxial tensions. The fully and two-step dynamic tensile tests were performed using a split Hopkinson bar. For the fully dynamic tensile tests, the strain rate for is controlled at 3000 s^{-1}. In the two-step dynamic tensile tests, the samples were first pre-formed at a strain rate of 1000 s^{-1}, and then fractured at a strain rate of 3000 s^{-1}.

From the test results, **Table 2** lists the ultimate tensile strength (UTS) and total fracture elongation (TFE) of the material under different tensile conditions. Under fully dynamic deformation, the material's UTS and TFE were 359 MPa and 45.1%, respectively. Under two-step dynamic deformation, the material's comprehensive mechanical properties were better than that under fully dynamic deformation. When the dynamic pre-strain was 16.7%, the material's UTS and TFE were 418 MPa an 54.1%, which increased by 16.4% and 20% compared to the fully dynamic deformation, respectively. The results indicated that dynamic pre-forming behavior can effectively enhance the material's strength and fracture elongation.

Table2 Mechanical properties of AA5A06 sheets under different tensile conditions

No.	Dynamic pre-strain level (%)	UTS (MPa)	TFE (%)	Tension pattern
T-1	/	359	45.1	Fully dynamic

T-2	16.7	418	54.1	Two-step dynamic

After the tensile tests, the fractures of the samples were analyzed from the view of microscopic, with observation conducted using a transmission electron microscope (TEM). Under fully dynamic deformation, distinct and uneven dislocation cells appeared, as shown in **Fig. 5a**. During dynamic deformation, plastic deformation tended to activate multiple slip systems. The multi-slip system activation and dislocation homogenization effect in dynamic deformation can form at higher plastic strain levels and strength. **Fig. 5b** shows the dark field image of the fracture. A large number of second-phase particles were fractured into two segments, and the sizes of cut particles exceeded 500 nm. Due to the severe fully dynamic deformation, the interactions between particles and dislocations were significantly enhanced.

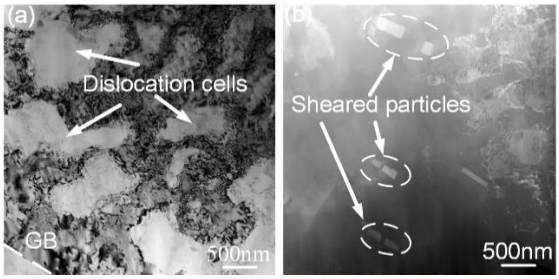

Figure 5*: Fully dynamic deformation (a) bright field image (b) dark field image*

As seen in **Fig. 6a**, the dislocation density within the grain boundaries (GBs) under two-step dynamic deformation was higher, and the sizes of dislocation cells were smaller. The entanglement and interaction between dislocations occurred more frequently, thus hindering dislocation movement and resulting in higher material strength. **Fig. 6b** shows a bright field image of dislocation entanglements. The dislocation distribution under two-step dynamic deformation was more uniform than that under fully dynamic deformation, indicating that two-step dynamic deformation contributed to a more homogeneous deformation, thereby exhibiting better plasticity. **Fig. 6c** shows the dark field image, a large number of fine second-phase particles were present, which may be the result of multiple cuts of the original second-phase particles due to two-step dynamic deformation. Firstly, the dynamic pre-forming caused interactions between the particles and the piled-up dislocations, leading to original particle cutting, similar to fully dynamic deformation. The second-step dynamic deformation was more intense with a wider range of dislocation pile-ups and greater dislocation multiplication, leading to a significant increase in stress concentration. As a result, the remaining particles were more easily cut in second-step dynamic deformation. The cumulative stress concentration from two steps made larger particles more susceptible to shear fracture. In **Fig. 6c**, there was sheared particle larger than 2500 nm in size.

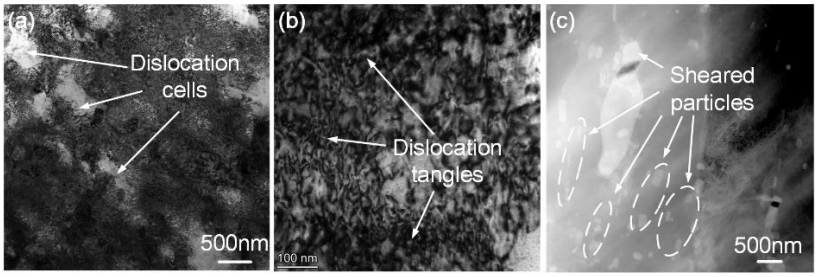

***Figure 6**: Two-step dynamic deformation (a), (b) bright field images (c) dark field image*

4 Conclusion

The following conclusions are drawn:

1. The EMIA method was proposed, and its feasibility was experimentally validated. Moreover, the process parameters for EMIA were optimized.
2. Compared to fully dynamic deformation, the strength and fracture elongation of the material were improved during two-step dynamic deformation.
3. The high dislocation density within GBs generated by two-step dynamic deformation resulted in higher material strength.
4. The material plasticity enhancement can be attributed to two factors. First, the dislocation distribution during dynamic deformation was uniform, preventing local strain concentration. Second, the original particles were sheared into two or more segments, and larger particles were more prone to fracture. The accumulated dislocations then cut through the particles, allowing them to continue moving, thereby releasing local shear stress.

References

Huang K.L., Ye H.T., Yu Z. F., Zhou X., 2022. *Energy absorption properties of composite sandwich tubes with pre-folded cores*. Composite Structures 294, pp. 115737.

Psyk, V., Risch, D., Kinsey, B.L., Tekkaya, A.E., Kleiner, M., 2011. *Electromagnetic forming – A review*. Journal of Materials Processing Technology 211 (5), pp. 787-829.

Cheng X., Yu H.P., 2025. *An incremental processing method for large thin-walled ring shells: Electromagnetic incremental assembly*. Journal of Manufacturing Processes 133, pp. 138-150.

Cui X.H., Mo J.H., Li J. J., Zhao J., Zhu Y., Huang L., Li Z.W., Zhong K., Zhao J., 2014. *Electromagnetic incremental forming (EMIF): A novel aluminum alloy sheet and tube forming technology*. Journal of Materials Processing Technology 214 (2), pp. 409-427.

Cheng X., Yu H.P., Lyu F., Jiang X., Zhong Y., 2025. *Mechanical properties and microstructure evolution of 5A06 aluminum alloy under two-step dynamic tension*. Materials Science & Engineering A 926, pp. 147958.